Lipid hydrogen isotope compositions primarily reflect growth water in the model archaeon *Sulfolobus acidocaldarius*

Carolynn M. Harris[a#], Sebastian Kopf[b], Jeemin H. Rhim[a,c], Alec Cobban[a], Felix J. Elling[d,e], Xiahong Feng[a], Jamie McFarlin[b,f], Yuki Weber[,d^], Yujiao Zhang[a%], Alice Zhou[a&], Harpreet Batther[b], Ann Pearson[d], William D. Leavitt [a,g]

[a] Department of Earth Sciences, Dartmouth College

[b] Department of Geological Sciences, University of Colorado at Boulder

[c] Department of Ecology, Evolution, and Marine Biology, U.C. Santa Barbara

[d] Department of Earth & Planetary Sciences, Harvard University

[e] Leibniz-Laboratory for Radiometric Dating and Isotope Research, Kiel University

[f] Department of Geology and Geophysics, University of Wyoming

[g] Department of Chemistry, Dartmouth College

Running head: Lipid hydrogen isotopes of S. acidocaldarius

Address correspondence to Carolynn M. Harris, carolynn.m.harris.gr@dartmouth.edu

[&] Current address: Connecticut Agricultural Experiment Station, New Haven, CT

[^] Current address: Chroma Medicine, Boston, MA

[%] Current address: National Center for Science & Technology Evaluation, P.R. China

Abstract

The stable hydrogen isotope composition (δ^2H) of lipid biomarkers can track environmental processes and remain stable over geologically relevant time scales, enabling studies of past climate, hydrology, and ecology. Most research has focused on lipids from the domain Eukarya (e.g., plant waxes, long-chain alkanes), and the potential of prokaryotic lipid biomarkers from the domain Archaea to offer unique insights into environments not captured by eukaryotic lipids remains unclear. Here, we investigate the H-isotope composition of biphytanes in *Sulfolobus acidocaldarius*, a model thermoacidophile and obligate heterotroph. We conducted a series of experiments that varied temperature, pH, shaking rate, electron acceptor availability, or electron donor flux. From these experiments, we quantified the lipid/water H-isotope fractionation ($^2\varepsilon_{L/W}$) values for core biphytane chains derived from tetraether lipids. The $^2\varepsilon_{L/W}$ values are consistently negative (-230 to -180 ‰) and are relatively invariant across all experiments despite a 20-fold change in doubling times and 2-fold change in lipid cyclization. The magnitude and relative invariance of $^2\varepsilon_{L/W}$ values are consistent with studies on other heterotrophic archaea and suggests archaeal lipids may be faithful recorders of the δ^2H composition of growth water. Our study highlights the potential of archaeal lipid δ^2H as a hydrological proxy, offering new insights into environments where traditional proxies, such as plant-derived lipids, are not available, including extreme environments and extraterrestrial settings.

Importance

Reconstructing past climates is crucial for understanding Earth's environmental history and its responses to changing conditions. This study examines *Sulfolobus acidocaldarius*, a thermoacidophilic archaeon that thrives in extreme environments like hot springs. These microorganisms incorporate hydrogen water in the growth environment into membrane lipids, creating hydrogen isotope signatures that can reflect hydroclimate conditions. Our findings show that these hydrogen isotope ratios remain consistent even under varying temperature, pH, oxygen levels, and electron donor fluxes, indicating a stable fractionation between lipids and water. This invariance suggests that *S. acidocaldarius* lipids could serve as a robust proxy for reconstructing ancient water H-isotope values, especially in extreme environments where traditional proxies, such as plant waxes, are absent. This research has broader implications for planetary-scale reconstructions, including potential applications in studying past climates on other planets, such as Mars, where similar microorganisms may have existed in hydrothermal conditions.

1. Introduction

The relative abundances of hydrogen isotopes ($^2H/^1H$) in water are set by physical, hydrological, and climatic factors (1, 2). Certain biomolecules incorporate these isotopes with a consistent offset (fractionation) relative to water, preserving a record of the isotopic composition (δ^2H values) of the water present during growth (3). Some lipids can retain their original H-isotope composition for up to 10^8 years and lipid hydrogen isotope compositions have been used to study hydrologic and environmental change over millennia to millions of years, dating as far back as the Paleoproterozoic (4–6). Most studies of biomarker H-isotope composition focus on lipids from photoautotrophic organisms (e.g., plant wax *n*-alkanes) or chemoautotrophic and heterotrophic bacteria (e.g., fatty acids) (3, 7–9) and the H-isotope compositions recorded in lipids from the Archaea are comparatively poorly understood. A small, but growing, body of literature, however, has begun to address this gap (10–15). Understanding the extent to which the δ^2H value of archaeal lipids records the δ^2H value of growth water requires a deeper examination of how environmental conditions impact this signal. A comprehensive investigation of the physicochemical factors affecting H-isotope fractionation between archaeal lipids and water ($^2\varepsilon_{L/W}$) is essential for employing archaeal lipid δ^2H composition as a proxy for the δ^2H composition of environmental water over space and time.

The $^2\varepsilon_{L/W}$ value for a biomolecule integrates both the composition of source water and the net biosynthetic fractionations resulting from the specific pathways used during lipid biosynthesis. Reported $^2\varepsilon_{L/W}$ values vary widely among domains of life. In phototrophic Eukaryotes (e.g., plants and algae), $^2\varepsilon_{L/W}$ values of waxes (e.g., n-alkanes) are consistently negative, ranging from -150 to -50 ‰ (8, 16). It is important to understand the causes of this variability when applying lipid δ^2H values to reconstruct water δ^2H values. Net biosynthetic fractionation is generally consistent across taxa, though genetic factors introduce some variance (17–22). Environmental factors such as temperature, salinity, light availability, and CO_2 concentration, also influence $^2\varepsilon_{L/W}$ values, possibly via their impact on growth and biosynthesis rates (16, 23–28). These effects are well-characterized in plants, and to a lesser extent in algae, and can be accounted for when the δ^2H values of plant waxes are used to reconstruct past hydroclimate (8, 29, 30).

In contrast to the coherent magnitude and direction of $^2\varepsilon_{L/W}$ values observed from phototrophic eukaryotes, the $^2\varepsilon_{L/W}$ of bacterial fatty acids varies widely in both direction and magnitude (-400 ‰ to +300 ‰) (31–38). Bacteria that use different central energy metabolisms (e.g., chemoautotrophy, photoautotrophy, or heterotrophy) exhibit distinct ranges of $^2\varepsilon_{L/W}$ values, which has been attributed to differences in metabolic pathways and the substrate used for growth (e.g., simple sugars vs. tricarboxylic acid (TCA) cycle intermediates). A recent study suggests that variations in $^2\varepsilon_{L/W}$ values from aerobic heterotrophic bacteria are explained by energy fluxes through the intracellular hydride carriers $NADP^+$ and NADPH (38). Given this metabolism-dependent heterogeneity, the δ^2H values of

bacterial lipids in sediment records may have more utility as proxies for the energetic state of past microbial metabolisms (33, 36, 38).

Lipid-water ^{2}H-fractionation from the domain Archaea have been understudied to-date. From what we do know, $^{2}\varepsilon_{L/W}$ values have been reported for diether lipids (archaeol) in a mesophilic halophile (11) and a methanogen (13), tetraether-derived biphytanes in three thermoacidophiles and one thermomesophile (10, 15), and one aerobic marine chemoautotroph (14), and whole tetraethers or tetraether-derived biphytanes in several environmental sediment samples (10, 12). The observed $^{2}\varepsilon_{L/W}$ values for these archaeal lipids are uniformly negative (i.e. -300 to -150 ‰) and similar in magnitude to those reported for isoprenoid lipids produced by eukaryotic phototrophs (e.g. C_{15} and C_{30} isoprenoids) (3, 25).

Our understanding of the factors controlling the H-isotope compositions of archaeal lipids are less developed than for the Eukarya and Bacteria. Recent experiments demonstrate that $^{2}\varepsilon_{L/W}$ is nearly constant over a range of growth rates in a marine autotroph (*Nitrosopumilus maritimus* (14)) and that the impacts of carbon metabolism and growth phase on $^{2}\varepsilon_{L/W}$ are minor (*Archaeoglobus fulgidus* (15)). This relative invariance in $^{2}\varepsilon_{L/W}$ values is perhaps surprising considering the taxonomic and metabolic diversity of the investigated Archaea. The impact of environmental factors on this fractionation, however, has only been investigated within a single archaeal strain (*Haloarcula marismortui* (11)). Further investigation of the effects of multiple environmental factors on $^{2}\varepsilon_{L/W}$ in Archaea is crucial, particularly since many archaea are adapted to extreme environments that can experience both rapid and large changes to physicochemical conditions (39).

Isoprenoid glycerol dibiphytanyl glycerol tetraethers (iGDGTs) are archaeal lipids with particular relevance to paleoenvironmental reconstructions (40). These tetraethers are structurally diagnostic, diagenetically robust, and routinely analyzed for paleoclimate reconstruction based on the relative abundances of specific structural moieties (40–42). Archaea can synthesize a unique series of iGDGTs that contain from zero to eight cyclopentane rings (e.g., iGDGT-0 through iGDGT-8), though the most highly ringed moieties (iGDGT-7 and -8) have only been recovered from hydrothermal spring environments (43). Members of the Thaumarchaeota phyla can also produce crenarchaeol, an iGDGT containing four cyclopentane rings and one cyclohexyl ring (43). The distribution of these moieties in natural systems is related to growth temperature and other environmental factors (44–48) and forms the basis of the TEX_{86} paleo sea surface temperature proxy (41). At low pH and high temperatures, Archaea synthesize more highly-ringed moieties as an adaptation to maintain membrane rigidity and reduce permeability. In hydrothermal systems, the ring distributions of thermoacidophilic archaea record the interactions between temperature, pH, energy availability, and other factors that influence growth rate (48–50).

To better understand the signals recorded by archaeal lipid δ^{2}H composition in natural systems, it is necessary to determine the extent to which environmental conditions influence $^{2}\varepsilon_{L/W}$ values. In this

study, we determined the H-isotope fractionation between iGDGT-derived biphytanes and growth water ($^{2}\varepsilon_{L/W}$) for the thermoacidophilic and heterotrophic archaeon, *Sulfolobus acidocaldarius* (DSM 639). *S. acidocaldarius* evolved to grow optimally under multiple extreme conditions, namely low pH's, high temperatures, and low oxygen partial pressure (51, 52). For this work *S. acidocaldarius* was selected as a model organism because it thrives in extreme environments devoid of traditional eukaryotic lipid proxies (e.g., plant waxes), and because it can grow under a wide range of physicochemical conditions, with rapid doubling times and high biomass yields (53).

Here we cultivated *S. acidocaldarius* over a range of physicochemical conditions that included shifts in temperature, pH, shaking rate, electron acceptor or electron donor flux. Changes in these environmental conditions are known to impact the growth rate and degree of iGDGT cyclization (47–49, 54, 55), but their impact on lipid/water fractionation is unexplored. Understanding how these environmental factors influence lipid/water fractionation is critical for interpreting archaeal lipid $\delta^{2}H$ signatures in natural systems and refining their use as robust proxies for reconstructing past hydroclimate conditions.

2. Methods

2.1 Culture strains and growth

Axenic cultures of *S. acidocaldarius* (DSM 639) were grown aerobically under different environmental conditions (**Table 1**). Culture media was prepared following the Brock recipe (56) with the following modifications (see *Substrate* column in Table 1). For all experiments, media contained 5.9 mmol L^{-1} (0.2% w/v) sucrose as the organic substrate. The electron donor flux experiments were also supplemented with 4.0 mmol L^{-1} (0.1% w/v) NZ-amine in addition to sucrose.

Growth was monitored photometrically at regular intervals throughout each experiment by measuring the optical density (i.e., absorbance at 1 cm pathlength) of a culture aliquot at 600 nm (OD_{600}) on a spectrophotometer. All experiments were inoculated to an initial OD_{600} between 0.004 and 0.008, using cells derived from an active pre-culture (grown on the same medium) in mid-exponential phase. Specific growth rates (division day^{-1}; μ) were calculated using OD_{600} measurements during the early to mid exponential phase after Cobban et al., (2020). Doubling time (T_D) was calculated as:

155 **Eq. (1)** $$T_D\ (hours) = ln(2)/\mu$$

156 **2.2 Experimental conditions experiments**

157 We examined how temperature, pH, shaking rate, O_2 availability, and electron donor (sucrose) flux
158 influence H-isotope fractionation in *S. acidocaldarius* through a series of batch, fed-batch, and
159 chemostat experiments.

160 **Batch experiments:** Three sub-experiments were performed in which one environmental condition
161 (temperature, pH, or shaking rate) was systematically varied while holding the other two conditions
162 constant (previously described in Cobban et al., 2020). The reference conditions were 70 °C, pH 3,
163 and 200 RPM shaking rate. Shaking rate is considered a proxy for aeration rate, where faster speeds
164 increase oxygen availability in the media, though it also increases physical agitation.

165 Batch experiments were performed in temperature-controlled, shaking incubators (Innova-42,
166 Eppendorf) in 250 mL Erlenmeyer flasks containing 125 mL media covered with loose plastic caps to
167 reduce evaporation. Evaporation was further reduced by maintaining a 2L tray of water in the
168 incubator to humidify the atmosphere. All experiments were performed in quintuplicate. Biomass
169 samples were collected in mid-exponential phase by centrifuging (3214 x *g*; Eppendorf 5810 R, S-4-
170 104 rotor) 50 mL of culture for 15 minutes at 4 °C, the resulting cell pellets were stored at -80 °C until
171 lipid extraction.

172 **Fed-batch bioreactor experiments:** To more precisely determine the impact of oxygen availability,
173 we performed gas-fed batch experiments in bioreactors (previously described in Cobban et al.,
174 2020). Briefly, *S. acidocaldarius* was grown in 300 mL of medium in 1 L glass vessels. To modulate
175 availability (as flux) of the terminal electron acceptor O_2 was introduced to bioreactors at four
176 different partial pressures: 0.2, 0.5, 2.0 or 20 % (balance N_2). The O_2 dry mixing ratios 0.2, 0.5, and
177 2% were generated by mixing pure N_2 mixed with 2% O_2 at 9:1, 3:1, and 0:1 ratios, respectively, which
178 was controlled via my-Control PID controllers (Applikon, Delft, Netherlands). The 20% experiment
179 used a separate gas feedstock of Ultra ZeroGrade Air (AirGas). Culture conditions were maintained
180 at 70 °C, pH 3, stirred at 200 RPM (Rushton-type impeller), and at a total gas flux of 200 mL min^{-1}.
181 Each experiment was performed in triplicate via three bioreactors operated in parallel. Biomass
182 samples were collected by removing culture directly from the vessel, centrifuged at 4 °C, to pellet
183 biomass, and then stored at -80 °C until lipid extraction.

184 **Chemostat experiments:** To determine the impact of electron donor flux, we performed chemostat
185 experiments in which the dilution rate of the growth vessel was set to yield cell doubling times (T_D) of
186 7.0, 21.3, and 40.0 hours (previously described in Zhou et al. 2020). Briefly, *S. acidocaldarius* was
187 grown in 300 mL of medium maintained at 70 ºC, pH 2.25, stirred at 200 RPM (Rushton-type
188 impeller), and aerated with a constant flux of 200 mL min^{-1} Zero Air (ultra-high purity, UHP, AirGas/
189 AirLiquide, Inc.). Three chemostats were operated in parallel under continuous culture conditions.

When steady state was achieved (assessed via regular OD_{600} measurements), biomass samples were harvested by continually collecting the outflow of each bioreactor into a chilled vessel (0 to 4 °C) for between 1 and 4 days, followed by centrifugation at 4 °C and storage at -80 °C prior to lipid processing. Multiple extracts representing 2 to 3 sampling events at identical growth rates were combined before lipid extraction.

2.3 Lipid extraction and derivatization

Core lipid fractions (iGDGTs) were extracted from lyophilized cell pellets via acidic hydrolysis-methanolysis (45, 48). iGDGTs were chemically derivatized to biphytanes to permit the determination of the δ^2H value of component biphytanes (10, 14). In brief, ether bonds were cleaved via digestion in 57% hydroiodic acid (HI) at 125 °C for 4 hours. The resulting alkyl iodides were hydrogenated (e.g., reduced to biphytanes, BPs) in H_2/PtO_2. An isotope dilution occurs when H is added during hydrogenation, which is corrected for during data processing and reduction (see Section 2.5).

2.4 Lipid identities & distributions

Isoprenoid BP chains were analyzed via GC-MS (Thermo ISQ LT with TRACE 1310) for compound identification and via GC-flame ionization detector (GC-FID; Thermo TRACE 1310) for compound quantification at the University of Colorado at Boulder Earth Systems Stable Isotope Lab (CUBES-SIL, Boulder, CO) (**FIG 1**). Biphytane yields and recovery were calculated using GC peak areas and co-injected n-alkane mixture as a quantification standard.

To describe the average amount of cyclopentyl rings in each BP distribution, we calculated a BP-Ring Index based on the relative abundance of each BP moiety (**Eq. 2**). This metric is similar to the iGDGT-based Ring Index (**Eq. 3**), which describes the average amount of cyclopentyl rings in a distribution based on the relative abundance of each iGDGT moiety (48, 57).

Eq. (2)

$$RI_{BP} = \frac{BP{-}1 + (2 \cdot BP{-}2) + (3 \cdot BP{-}3)}{\sum_o^3 BP}$$

Eq. (3)

$$RI_{GDGT} = \frac{iGDGT{-}1 + (2 \cdot iGDGT{-}2) + (3 \cdot iGDGT{-}3) + \ldots + (8 \cdot iGDGT{-}8)}{\sum_o^8 iGDGT}$$

2.5 δ^2H analysis of media waters, substrates, and biphytane lipids

2.5.1 Media waters

Water samples for hydrogen isotope (δ^2H) analysis were collected concurrently with harvesting biomass for lipid analyses. Aliquots of filter-sterilized growth medium water was measured for δ^2H at the Stable Isotope Laboratory at Dartmouth College via a dual inlet isotope ratio mass spectrometer (IRMS; Thermo Delta Plus 304 XL) coupled to an H-Device (pyrolyzed to H_2 gas) for water reduction by chromium powder at 850°C (previously described in Kopec et al. (2018). The δ^2H_{Water} values were corrected using three laboratory standards spanning -161 to -7 ‰ vs. VSMOW, which were run every 8-10 samples. Analytical precision was <0.5 ‰.

2.5.2 Substrates

The δ^2H composition of non-exchangeable C-bound H from substrates used in growth media was analyzed in triplicate as trifluoroacetate derivatives via a Thermo Delta Plus XP coupled to a TC-EA (58). The δ^2H composition of sucrose was -93.0 ± 1.2 ‰.

2.5.3 Biphytanes

For all experiments, we report $^2\varepsilon_{L/W}$ values for biphytane (BP) hydrocarbons derived via ether cleavage from acid extractable iGDGTs. The δ^2H composition of individual BPs was determined by gas chromatography pyrolysis isotope ratio mass spectrometry (GC-P-IRMS) on a GC IsoLink II IRMS System (Thermo Scientific) at the University of Colorado at Boulder Earth Systems Stable Isotope Lab (CUBES-SIL, Boulder, CO). The system comprised a Trace 1310 GC fitted with a programmable temperature vaporization (PTV) injector and either a 30 m ZB5HT column (i.d. = 0.25 mm, 0.25 µm, Phenomenex, Torrance, CA, USA) or a 60 m DB1 column (i.d. = 0.25 mm, 0.25 µm, Agilent, Santa Clara, CA, USA), ConFlo IV interface, and 253 Plus mass spectrometer (Thermo Scientific).

2.5.4 Data reduction and notation

The δ^2H values of individual biphytanes (δ^2H_{BP}) were measured relative to H_2 reference gas (δ^2H_{raw}) and calibrated to the international references scale (VSMOW) using a standard n-alkane mixture (A7, containing C15 through C30 n-alkanes spanning -9 to -263 ‰ vs. VSMOW; A. Schimmelmann, Indiana University). The A7 standard was combined with a C_{36} n-alkane (nC_{36}, -259.2 ‰ vs. VSMOW; A. Schimmelmann, Indiana University) and measured throughout each analytical run at regular intervals and at different concentrations. The BP hydrogen isotope calibration was performed as in Leavitt et al., (2023) using the R packages *isoreader* (v 1.3.0) and *isoprocessor* (v 0.6.11) available at github.com/isoverse (59). In brief, δ^2H_{raw} values were corrected for offset, scale compression and peak-size effects using an inverted multivariate linear regression which was applied to all standards and samples to determine δ^2H_{cal} values. Further details of calibration and data reduction are available in Leavitt et al., 2023. The total analytical uncertainty of the corrected δ^2H_{BP} values was calculated using standard error propagation of the peak-size adjusted error estimates and hydrogenation correction assuming all errors to be uncorrelated. The hydrogenation correction ranged from 10.3 to 12.7 ‰ and increased analytical uncertainty by up to 1.9 ‰.

All $^2H/^1H$ ratios are reported in delta notation (δ^2H) in permil (‰) units relative to the international seawater standard on the VSMOW-SLAP (Vienna Standard Mean Ocean Water, Standard Light Antarctic Precipitation) scale.

Eq. (4)

$$\delta^2H\ (‰) = \left(\frac{^2H/\ ^1H_{Sample}}{^2H/\ ^1H_{Standard}} - 1\right)$$

All fractionation factors are reported in epsilon notation ($^2\varepsilon$) in permil (‰) units. The hydrogen isotope fractionation between growth water and BP lipids ($^2\varepsilon_{L/W}$) is calculated as:

Eq. (5 a, b)

$$^2\alpha_{L/W} = \frac{^2H/\ ^1H_{BP}}{^2H/\ ^1H_{Water}}$$

$$^2\varepsilon_{L/W}\ (‰) = (\ ^2\alpha_{L/W} - 1)$$

Corrected δ^2H_{BP} values and resulting $^2\varepsilon_{L/W}$ fractionation factors from biological replicates (n ≥ 1) and analytical replicates (n ≥ 3) were averaged for each experimental condition. All averages are weighted means of individual measurements ($1/\sigma^2$ weights) to account for the amplitude-dependent range in uncertainties. The reported error estimate of each average is the larger of the standard deviation of all replicates or the propagated uncertainty from individual measurements. Abundance weighted averages for δ^2H_{BP} and $^2\varepsilon_{L/W}$ values include all BPs with relative abundance > 5%.

The ring difference ($\Delta\varepsilon$/ring), or changes in $^2\varepsilon_{L/W}$ with increasing number of ring structures is calculated for all pairwise combinations of $^2\varepsilon_{L/W}$ values after Leavitt et al., (2023) where X and Y refer to the ring number of BP moieties and X > Y:

Eq. (6)

$$\frac{\Delta\varepsilon}{ring}(‰) = \frac{^2\varepsilon_{L/W}(X) - \ ^2\varepsilon_{L/W}(Y)}{(X-Y)}$$

Raw data and code for all data manipulations and statistical analyses is available on GitHub (https://github.com/carolynnharris/Saci_Enviro_d2H) and archived on Zenodo (60)

3. Results

We examined how temperature, pH, shaking rate, O_2 availability, and electron donor (sucrose) flux influence H-isotope fractionation in *S. acidocaldarius* through a series of batch, fed-batch, and chemostat experiments. Details of the growth responses and lipid iGDGT profile responses to these conditions can be found in Cobban et al., (2020) and Zhou et al., (2019). In brief, each environmental condition independently influences growth rate, the relative abundance of many subsets of iGDGT core lipids, and the RI-GDGT (47, 48) (**Table 1, FIG 2A-E, S1**).

Here, we show that each environmental condition also influences the relative abundance of BP lipids and the RI-BP (**Table 2**, **FIG. 2F-O**). Among all samples, the relative abundance of biphytanes

averaged 13%, 30%, 49%, 7% for BP-0, -1, -2, and -3, respectively; BP-3 was the least abundant and was not measurable in some samples. RI-BP ranged from 1.01 to 2.04 and, as expected, was positively correlated with RI-GDGT (R^2 = 0.52, p = 0.001, **FIG. S2**). Among all samples, the abundance weighted mean δ^2H_{BP} values range from -276 to -225 ‰ and were consistently depleted in ^2H relative to growth water, corresponding to $^2\varepsilon_{L/W}$ values from -230 to -180 ‰ (**Table 2, FIG. 2P-T**).

Despite significant effects on growth rate and lipid cyclization, individual environmental parameters had minimal impact on $^2\varepsilon_{L/W}$ values, which spanned a range of 44, 31, 15, 21, and 25 ‰ in the temperature, pH, shaking rate, O_2 availability, and electron donor flux experiments, respectively. We observed a weak linear relationship between environmental conditions and $^2\varepsilon_{L/W}$ only in the electron donor flux experiment, where larger doubling times are associated with slightly less negative $^2\varepsilon_{L/W}$ values (smaller offset from water) (R^2 = 0.89, p = 0.22, slope = 0.72 ± 0.25 ‰/ hour) (**FIG. 2T**).

In the batch and fed-batch experiments, $^2\varepsilon_{L/W}$ values for individual BPs showed no consistent pattern with increasing number of cyclic moieties and the ring difference (Δε/ring) varied widely in direction and magnitude among all treatments (-39 to +24 ‰) (**Table 2**, **FIG. 3A-D, S3A-D**). The variability in mean Δε/ring was smaller, though still not of uniform direction, with values ranging from -5.4 to +10.2 ‰ (**Table 2, FIG. S4A-D**). In contrast, $^2\varepsilon_{L/W}$ values in the chemostat experiment generally increased with the number of cyclic moieties, showing offsets of 3.7, 4.1, and 10.1 ‰ for BP-1, BP-2, and BP-3 relative to BP-0 (**Table 2, FIG. 3E, S3E**). Similarly, the mean ring difference (Δε/ring) was uniformly positive and showed little variation among doubling times, ranging from 4.9 to 9.2 ‰ (**Table 2, FIG. S4E**). On average in continuous culture, each additional ring contributes a 7.4 ± 2.2 ‰ increase to biphytane $^2\varepsilon_{L/W}$.

Correlation matrices show the linear relationship between each environmental condition, growth parameters (doubling time and maximum OD_{600}), mean lipid cyclization indices (RI-BP and RI-GDGT), Δε/ring and abundance weighted $^2\varepsilon_{L/W}$ values for each environmental condition experiment (**FIG. 4**). These plots further demonstrate that the minimal variation in $^2\varepsilon_{L/W}$ observed within each experiment is not related to variation in the experimentally manipulated environmental conditions or any other measured parameter.

To explore the possibility that lipid/water fractionation is related to optimal growth, we relate abundance weighted mean $^2\varepsilon_{L/W}$ values to doubling time for each environmental condition (**FIG. 5A-E**). To allow for comparisons among all environmental conditions, we also relate $^2\varepsilon_{L/W}$ to doubling time for all experiments combined. In this pooled dataset, abundance weighted mean $^2\varepsilon_{L/W}$ values range from -230 to -180 ‰ (mean = -204 ± 12 ‰, based on 22 biological replicates; **Table 2**) and showed no correlation to doubling time (**FIG. 5F**, R^2 = 0.0, p = 0.97), indicating a decoupling between lipid/water fractionation and growth rate.

316 **4. Discussion**

317 **4.1 Effect of environmental conditions on archaeal lipid $^2\varepsilon_{L/W}$ values**

318 The primary goal of this work was to investigate the impact of environmental conditions on
319 lipid/water fractionation in archaeal lipids, which relates to their potential as archives of
320 hydroclimate across space and time. The conditions tested in this study were chosen to encompass
321 the natural conditions of thermoacidophilic archaea, which are globally distributed in hot, acidic
322 features including fumaroles (steam saturated discharges) as geysers and pools in the terrestrial
323 environment, and hydrothermal vents in the marine environment (61). Both realms experience steep
324 and rapidly changing gradients in temperature, pH, oxygen, and dissolved solute concentrations,
325 which can disturb ecological niches (62). As a result, Archaea have adapted to or evolved strategies
326 to mitigate these challenges (61, 63).

327 In *S. acidocaldarius*, our experimental manipulations of temperature, pH, shaking rate, electron
328 acceptor (O_2) availability, and electron donor (sucrose) flux elicited a 20-fold change in growth rate
329 and 2-fold change in mean biphytane cyclization (RI-BP), but $^2\varepsilon_{L/W}$ values were largely invariant (-204
330 ± 12 ‰, n = 22). This finding is consistent with previous studies that show archaeal lipids are
331 consistently ^{2}H-depleted relative to source water and display a narrow range of $^2\varepsilon_{L/W}$ values despite
332 considerable variation in taxonomy, metabolic mode, and growth conditions (10–15) (**FIG 6**).

333 In heterotrophic archaea, lipid-bound H can originate from water or the organic substrate used for
334 growth, with intracellular hydride carriers, such as NADPH, mediating the incorporation of H from
335 both sources into lipids (11, 33, 38). In heterotrophs, the NADPH incorporated into lipid products
336 inherits some H from the available organic substrate(s). While there are several potential
337 mechanisms by which each environmental stressor tested here could influence lipid/water
338 fractionation in archaea, our data suggest these processes either do not occur or are insufficient to
339 cause a measurable effect. Temperature, pH, oxygen levels, and nutrient availability are known to
340 trigger physiological responses in archaea, including changes in growth rates, membrane lipid
341 composition, and enzyme activity (47, 48, 52, 64). Enzyme kinetics, which are influenced by growth
342 temperature and oxidative stress (65), could affect lipid/water fractionation if the enzyme catalyzing
343 hydrogen transfer is associated with a significant isotope effect (33). High temperatures and low pH
344 reduce water exchange across archaeal membranes to prevent osmotic stress (64), which could
345 enrich the intracellular water in ^{2}H and potentially reduce apparent lipid/water fractionation (66).
346 Additionally, changes in electron donor availability can shift the pathway by which NADPH is
347 reduced, which could influence the δ^2H composition of NADPH, which ultimately supplies protons
348 to lipid products (67, 68). For example, methanogenic archaea switch between the reductive acetyl-
349 CoA and F_{420}-dependent hydrogenase systems depending on if electron donors (H_2 or formate) are
350 abundant or limiting (67). Despite these possible mechanisms, lipid/water fractionation in *S.*
351 *acidocaldarius* remains largely invariant in each experiment, indicating that these processes either

352 do not occur or are not significant enough to alter fractionation under the tested conditions. An
353 alternative hypothesis is that *S. acidocaldarius* maintains a constant internal metabolic balance,
354 particularly in NADPH production and utilization, regardless of external conditions.

355 Physiological responses to stressors impact growth rate and examining $^{2}\varepsilon_{L/W}$ values in response to
356 optimal vs. suboptimal growth may provide a more coherent explanation for the non-linear patterns
357 we observe across the environmental conditions tested. The $^{2}\varepsilon_{L/W}$ values for *S. acidocaldarius*,
358 however, are not correlated to growth rate in any single environmental condition experiment or when
359 data for all conditions are pooled. This finding suggests that cells maintain stable internal metabolic
360 processes resulting in a consistent H-balance over a range of growth rates and is consistent with the
361 theory that a constant lipid/water fractionation is a feature of an imperturbable central energy
362 metabolism (14, 15). *S. acidocaldarius*, like most archaea, employs energy-efficient metabolic
363 strategies (69, 70), possibly as an adaptation to energy-limiting environments (63, 71). In tightly
364 controlled metabolic pathways, the balance between supply and use of NADPH reducing power
365 appears to remain constant, even under energy-stress conditions. Previous research suggests
366 archaea may exist in a permanent state of NADPH deficiency such that all NADPH is immediately
367 used for biosynthesis with little to no flux from NADPH back to NADH (14). This efficiency in NADPH
368 use may explain why changing growth rates do not impact kinetic isotope effects associated with
369 biosynthesis and hydride exchange. NADPH deficiency (deemed NADPH flux imbalance by Wijker et
370 al., 2019) is associated with energy limitation, and can provide a framework to relate patterns in $^{2}\varepsilon_{L/W}$
371 values to the fluxes of H through dehydrogenase and transhydrogenase enzymes. Indeed, NADPH
372 flux imbalance may explain why all archaea (to-date) and autotrophic and obligately anaerobic
373 bacteria display negative $^{2}\varepsilon_{L/W}$ values of similar magnitude (15, 33, 36, 38). This similarity is striking
374 given that fatty acids and isoprenoid GDGTs are formed via different biosynthetic pathways and
375 suggests that the ultimate control on $^{2}\varepsilon_{L/W}$ values may be related to free energy yields (15).

376 Both the O_2 availability and sucrose flux experiments test the hypothesis that energy limitation –
377 either terminal electron acceptor or donor – can alter $^{2}\varepsilon_{L/W}$ values in archaea. These experiments
378 produced the largest range in doubling times (2 to 50 hours and 7 to 44 hours in the O_2 availability
379 and electron donor experiments, respectively); yet $^{2}\varepsilon_{L/W}$ values remained fairly consistent (-217 to -
380 196 ‰ and -276 to -244 ‰, respectively). *N. maritimus* is the only other archaeon in which the
381 relationship between electron donor (ammonium) flux and lipid/water fractionation was examined;
382 this archaeon similarly exhibited no significant correlation between a three-fold change in doubling
383 time and $^{2}\varepsilon_{L/W}$ values ($R^2 = 0.22$, $p = 0.07$, slope = 0.18 ± 0.09 ‰/ hour) (14). The authors speculate
384 this strain maintains a consistent H-balance over a range of electron donor fluxes as an adaptation
385 that allows cells to perform nitrification with energy-efficient CO_2 fixation in oligotrophic
386 environments (14). These findings suggest that archaea with diverse physiologies (e.g., heterotrophy
387 vs. chemoautotrophy, extremophily vs. mesophily) maintain a constant lipid-to-water fractionation
388 that is minimally affected by free energy availability and may reflect the fact that Archaea are
389 adapted to chronic energy limitation (63, 71). This stability may reflect tightly regulated physiological

390 processes, such as isoenzyme switching and modulation of enzyme activities, which help maintain
391 metabolic homeostasis under both optimal and sub-optimal growth conditions (72). In contrast, in
392 bacteria and some planktonic eukaryotes faster growth is associated with larger lipid/water
393 fractionation (66, 73, 74) and $^{2}\varepsilon_{L/W}$ values for Bacteria are influenced by electron donor flux (33, 36,
394 38).

395 The only other study in archaea to examine the relationship between environmental conditions and
396 lipid/water fractionation cultured the halophilic heterotrophic archaeon, *H. marismortui* (which
397 produces archaeol diethers), under varying temperatures and salinities when grown on complex rich
398 medium (11). The resulting $^{2}\varepsilon_{Archaeol/W}$ values are relatively invariant (ranging from -126 to -143 ‰;
399 more enriched than our observations for *S. acidocaldarius*) and are decoupled from growth rate (**FIG.**
400 **S5;** R^2 = 0.07, p = 0.7, slope = 0.85 ± 1.84 ‰ / hour), providing more evidence that archaea maintain
401 a stable internal H-balance across a range of growth conditions (11).

402 The impact of growth phase on H-isotope dynamics has not been studied in depth. The batch and
403 fed-batch experiment techniques used here for *S. acidocaldarius* and in the *H. marismortui* study
404 integrate across growth stages, whereas the chemostat electron donor flux experiments for *S.*
405 *acidocaldarius* and *N. maritimus* achieve constant growth rates. A recent study grew *A. fulgidus* in
406 batch cultures and found that $^{2}\varepsilon_{L/W}$ values were more depleted (larger offset from water) during
407 exponential phase relative to stationary phase (15). This pattern was consistent between
408 heterotrophic and autotrophic experiments. The culture conditions in Rhim et al. resulted in a
409 threefold difference in growth rates (similar change to the *N. maritimus* study, but much smaller
410 range than the 20-fold change we report for *S. acidocaldarius* here) and a 50 ‰ change in $^{2}\varepsilon_{L/W}$ values
411 (-280 ‰ to -230 ‰). Rhim and coauthors conclude that both metabolic mode (heterotrophic vs.
412 autotrophic growth) and growth phase impact $^{2}\varepsilon_{L/W}$ values, though the total variance among all
413 treatments was small and overlaps which ranges reported for other archaea (15).

414 **4.2 Effect of biphytane ring number on archaeal lipid $^{2}\varepsilon_{L/W}$ values**

415 Stoichiometric modeling predicts that BPs with more rings incorporate less of the highly-
416 fractionated hydrogen donated through GGR reduction, a process where the enzyme geranyl-geranyl
417 reductase (GGR) catalyzes the reduction of double bonds in isoprenoid chains, thereby affecting the
418 isotopic composition of the resulting lipids (14). Interestingly, in our *S. acidocaldarius* work, this
419 stepwise enrichment is only seen in the chemostat experiments, where each additional ring
420 contributes 7.4 ± 2.2 ‰ to biphytane $^{2}\varepsilon_{L/W}$ values. In the batch and fed-batch experiments, there is
421 no consistent dependence of $^{2}\varepsilon_{L/W}$ values on the number of biphytane moieties. In particular, the
422 Δε/ring trends differ between the shaking rate and O_2 availability experiments, which likely reflects
423 the fact that shaking rate can also impart stress via physical agitation in addition to increasing
424 oxygenation of microbial media (47).

iGDGT-derived BPs extracted from marine sediments also lack a clear stepwise enrichment with increasing ring moieties (10), but this likely occurs because sediments integrate lipids synthesized by different populations of archaea that are either growing on multiple substrates or in different water masses (10). It is less clear why the pure *S. acidocaldarius* batch and fed-batch cultures do not display a ring-specific pattern, though it perhaps relates to variations in biosynthetic fractionations accompanying changes in lipid biosynthesis across the growth phases (44). Considering all the available data, this enrichment pattern appears only minimally affected by differences in growth rate and metabolism, as the magnitude of per-ring increase in $^{2}\varepsilon_{L/W}$ value is similar for *Sulfolobus* sp. (10), *S. acidocaldarius* (chemostat experiment in this study), and *N. maritimus* (14), which collectively represent a 5-fold range of growth rates, and a variety of metabolisms and carbon substrates (*Sulfolobus* sp. = yeast extract + O_2; *S. acidocaldarius* = sucrose + O_2; *N. maritimus* = chemoautotroph on NH_4 + O_2). The magnitude of this stepwise enrichment, however, is small and would likely have a minor impact (usually < 10 ‰) on the abundance weighted mean $^{2}\varepsilon_{L/W}$ value even in cases where the BP Ring Index was markedly different among samples.

4.3 Archaeal lipid $^{2}\varepsilon_{L/W}$ as a function of central metabolism

The *S. acidocaldarius* $^{2}\varepsilon_{L/W}$ values we report are broadly similar to results from previous experimental investigations of the *Sulfolobus* genus cultured heterotrophically. When grown at 75 °C and pH 2 on yeast extract, a *Sulfolobus* strain displayed $^{2}\varepsilon_{L/W}$ values from -213 to -161 ‰ for BP-0 to -4 (abundance weighted mean = -180 ‰ (10) vs. -204 ± 12 ‰ for *S. acidocaldarius* here). In another study, *Sulfolobus solfataricus* grown at 76 °C and pH 3.5 on glutamate displayed more enriched $^{2}\varepsilon_{L/W}$ values, averaging -134 ‰ when intact iGDGT-1 and -2 were analyzed (12). The difference in $^{2}\varepsilon_{L/W}$ values may in part be due to the structures analyzed. Lengger and colleagues analyzed intact iGDGTs including the glycerols which may enrich the $\delta^{2}H_{iGDGT}$ composition, though the different substrate may also play a role (12). Glutamate, an amino acid, is a more complex substrate than simple sugars (such as sucrose) and primarily enters the *Sulfolobus* central metabolism through the TCA cycle (75). Simple sugars enter metabolism primarily through the Entner-Doudoroff pathway, which converts the sugar to intermediates that feed into the TCA cycle (75).

When *S. acidocaldarius* is grown heterotrophically on a simple sugar (glucose), the weighted mean $\delta^{2}H$ composition of biphytane lipids is strongly correlated with $\delta^{2}H_{Water}$, indicating a strong first-order control (see *Supplementary Materials*, **FIG. S6**). A simple isotope mass balance model (**Eq. S1**) suggests water contributes at least 56 ± 1% of the total H flux to lipids (**FIG. S7**). Further experimental work and complementary isotope flux models are needed to determine the specific pathways (and associated isotope effects) used during iGDGT synthesis in *S. acidocaldarius* (76).

Autotrophic archaea that produce iGDGTs, however, source their entire H budget to lipids from water in the growth environment and show more negative $^{2}\varepsilon_{L/W}$ values than those we observe for *S. acidocaldarius*. In the marine chemoautotroph, *N. maritimus*, grown in continuous culture, BP/water

fractionation ranged from -272 to -260 ‰ (14). Similarly, BP/water fractionations for a metabolically-flexible archaeon, *Archaeoglobus fulgidus*, ranged from -280 to -226 ‰ when cultured with several unique carbon substrates and electron donor/acceptor pairs (15). This difference may be driven by the distinct metabolic modes used (e.g., autotrophy vs. heterotrophy) and/or by unique metabolic pathways that employ various intracellular hydride carriers and reductants to bring H's to the lipid sites, which could generate different net biosynthetic fractionations. Metabolic flux models suggest that in autotrophic archaea (e.g., *N. maritimus*), H-isotope fractionation due to the electron transport chain and NADPH generation result in more depleted lipids than for heterotrophic archaea, such as *Sulfolobus* species, because the source of NADPH impacts $^{2}\varepsilon_{L/W}$ values (14). In both heterotrophic and aerobic archaea, most NADPH is generated by glucose dehydrogenase and potentially glyceraldehyde dehydrogenase from the Entner-Doudoroff pathway (72, 77).

Overall, the range of $^{2}\varepsilon_{L/W}$ values in Archaeal lipids is narrower than the ranges observed in Bacteria or Eukarya (**FIG. 6**). While the sample size for Bacteria and Eukarya are two-fold and four-fold larger than for Archaea, respectively, Bartlett's test for homogeneity of variances confirm that Archaeal $^{2}\varepsilon_{L/W}$ values have smaller variance compared to Eukarya ($K^2_{(1)} = 16.4$, $p < 0.0001$) and Bacteria ($K^2_{(1)} = 118.5$, $p < 0.0001$) after accounting for sample size. Reported $^{2}\varepsilon_{L/W}$ values for bacterial fatty acids vary over 600 ‰ and include large negative and large positive values (15, 33, 36, 38, 78). In Eukarya, $^{2}\varepsilon_{L/W}$ values are uniformly negative and span over 300 ‰, though certain lipid classes group together (3, 25, 79). Lipids that are formed via the same biosynthetic pathway (e.g., acetogenic or isoprenoid pathway) tend to occupy distinct ranges of $^{2}\varepsilon_{L/W}$ (15). Isoprenoid lipids produced via the MVA pathway in eukaryotes have similar $^{2}\varepsilon_{L/W}$ values to iGDGT-derived biphytanes in archaea (15). This similarity suggests that the MVA pathway used for isoprenoid lipid biosynthesis has a large net fractionation in both domains of life.

4.4 Applications and Conclusion

Our calibration of biphytane δ^2H composition as a proxy for the δ^2H of environmental water in *S. acidocaldarius* has significant implications for paleohydroclimate and paleoecology reconstructions. First, this calibration may enable hydroclimate factors like precipitation, elevation, and seasonality to be reconstructed for environments that do not contain traditionally analyzed lipid biomarkers (e.g., plant waxes) – this includes extreme environments that do not support plant growth (e.g., terrestrial hydrothermal systems, salars, and hyperarid regions). Archaeal lipid δ^2H values will be most powerful as a proxy in cases where a single-substrate source is a reasonable assumption.

Second, biphytane δ^2H composition could be applied to marine or lacustrine sedimentary archives where multiple sources of organic matter are suspected, such as a mix of plant waxes representing *in situ* marine/ aquatic production and allochthonous terrestrial production (e.g., aeolian deposition). In this case, plant wax δ^2H values would reflect a mixture of growth waters (marine/lake water and soil water). In contrast, iGDGTs are likely derived solely from archaea living in the overlying

water column with few potential terrestrial sources and thus the δ^2H composition of iGDGTs would only reflect marine/lake water (42).

Here, we show that in the model thermoacidophile *S. acidocaldarius* grown on simple sugars, lipid-water fractionation ($^2\varepsilon_{L/W}$) is not dependent on any of the environmental conditions tested or on growth rate. This finding suggests that *S. acidocaldarius* may have evolved stable metabolisms that exist in a constant NADPH deficit, possibly reflecting adaptation to energy-limiting environments. We conclude that *S. acidocaldarius* will likely demonstrate reliably invariant lipid/water fractionation regardless of growth rate, nutrient status, or energy availability, and that lipid/water fractionation may be more constant for certain archaeons than for phototrophic eukaryotes. For both domains, however, there is more variability in lipid/water fraction relative to the spatial and temporal variability in precipitation δ^2H values, and more research is needed to understand the sources of this variation so that it can be accounted for in proxy applications.

This calibration underscores the potential for archaeal lipid δ^2H composition as a proxy for past hydroclimates that could complement or be used independently of eukaryotic lipid δ^2H composition. Future research should focus on exploring the effects of growth phase and metabolic pathways on lipid/water fractionation in *S. acidocaldarius* and other archaeal species. Expanding these investigations to include more diverse environmental conditions, such as varying carbon substrates or mixed microbial communities, could further validate the consistency of $^2\varepsilon_{L/W}$ values and refine its utility as a hydrological proxy. Integrating isotope flux models with experimental data such as those generated here, will allow us to better elucidate the specific biochemical pathways responsible for the observed fractionation patterns in domain Archaea.

Acknowledgements

This research was supported by research grant NSF EAR #1928303940 (WDL, SHK); Simons Foundation Award #623881 (WDL); Dartmouth College (WDL); National Aeronautics and Space Administration (NASA) New Hampshire Space Grant (NASA-SSW-80NSSC19K0539); Deutsche Forschungsge-meinschaft grant 441217575 (F.J.E.). The authors thank the CU Boulder Earth Systems Stable Isotope Lab (CUBES-SIL) Core Facility (RRID:SCR_019300) for analytical contributions; B. Chiu (then at Dartmouth), J. Blewett (then at Harvard), S. Carter (Harvard), and A. Maloney (CU Boulder) for expert laboratory support; Simon D. Kelly from International Atomic Energy Agency, Vienna for measuring the δ^2H composition of carbon substrates; and all members of the Leavitt lab for all their support.

528 **References**

529 1. Gat JR. 1996. Oxygen and hydrogen isotopes in the hydrologic cycle. Annual Review of Earth
530 and Planetary Sciences 24:225–262.

531 2. Hayes JM. 2001. Fractionation of carbon and hydrogen isotopes in biosynthetic processes.
532 Stable Isotope Geochemistry 43:225–277.

533 3. Sessions AL, Burgoyne TW, Schimmelmann A, Hayes JM. 1999. Fractionation of hydrogen
534 isotopes in lipid biosynthesis. Organic Geochemistry 30:1193–1200.

535 4. Sessions AL, Sylva SP, Summons RE, Hayes JM. 2004. Isotopic exchange of carbon-bound
536 hydrogen over geologic timescales. Geochimica et Cosmochimica Acta 68:1545–1559.

537 5. Dawson D, Grice K, Wang SX, Alexander R, Radke J. 2004. Stable hydrogen isotopic
538 composition of hydrocarbons in torbanites (Late Carboniferous to Late Permian) deposited
539 under various climatic conditions. Organic Geochemistry 35:189–197.

540 6. Love GD, Zumberge JA. 2021. Emerging Patterns in Proterozoic Lipid Biomarker Records, 1st
541 ed. Cambridge University Press.
542 https://www.cambridge.org/core/product/identifier/9781108847117/type/element. Retrieved
543 22 March 2024.

544 7. Liu J, An Z. 2019. Variations in hydrogen isotopic fractionation in higher plants and sediments
545 across different latitudes: Implications for paleohydrological reconstruction. Science of The
546 Total Environment 650:470–478.

547 8. McFarlin JM, Axford Y, Masterson AL, Osburn MR. 2019. Calibration of modern sedimentary
548 δ2H plant wax-water relationships in Greenland lakes. Quaternary Science Reviews
549 225:105978.

550 9. Ladd SN, Nelson DB, Bamberger I, Daber LE, Kreuzwieser J, Kahmen A, Werner C. 2021.
551 Metabolic exchange between pathways for isoprenoid synthesis and implications for
552 biosynthetic hydrogen isotope fractionation. New Phytologist 231:1708–1719.

553 10. Kaneko M, Kitajima F, Naraoka H. 2011. Stable hydrogen isotope measurement of archaeal
554 ether-bound hydrocarbons. Organic Geochemistry 42:166–172.

555 11. Dirghangi SS, Pagani M. 2013. Hydrogen isotope fractionation during lipid biosynthesis by
556 Haloarcula marismortui. Geochimica et Cosmochimica Acta 119:381–390.

557 12. Lengger SK, Weber Y, Taylor KWR, Kopf S, Berstan R, Bull I, Mayser J, Leavitt WD, Blewett J,
558 Pearson A, Pancost RD. 2020. Determination of the d2H values of high molecular weight lipids

559 by high temperature GC coupled to isotope ratio mass spectro. Rapid Communications in
560 Mass Spectrometry.

561 13. Wu W, Meador TB, Könneke M, Elvert M, Wegener G, Hinrichs K. 2020. Substrate-dependent
562 incorporation of carbon and hydrogen for lipid biosynthesis by Methanosarcina barkeri.
563 Environmental Microbiology Reports https://doi.org/10.1111/1758-2229.12876.

564 14. Leavitt WD, Kopf SH, Weber Y, Chiu B, McFarlin JM, Elling FJ, Hoeft-McCann S, Pearson A.
565 2023. Controls on the hydrogen isotope composition of tetraether lipids in an autotrophic
566 ammonia-oxidizing marine archaeon. Geochimica et Cosmochimica Acta 352:194–210.

567 15. Rhim JH, Kopf S, McFarlin J, Maloney AE, Batther H, Harris CM, Zhou A, Feng X, Weber Y,
568 Hoeft-McCann S, Pearson A, Leavitt WD. 2024. Metabolic imprints in the hydrogen isotopes of
569 Archaeoglobus fulgidus tetraether lipids. Geochimica et Cosmochimica Acta 386:196–212.

570 16. Sachs J. 2014. Hydrogen Isotope Signatures in the Lipids of Phytoplankton, p. 79–94. *In*
571 Treatise on Geochemistry. Elsevier.

572 17. Gao L, Edwards EJ, Zeng Y, Huang Y. 2014. Major Evolutionary Trends in Hydrogen Isotope
573 Fractionation of Vascular Plant Leaf Waxes. PLoS ONE 9:e112610.

574 18. Bender, Suess, Chitwood, Bradley. 2016. Investigating genetic loci that encode plant-derived
575 paleoclimate proxies, p. PP24B-03. *In* .

576 19. Baan J, Holloway-Phillips M, Nelson DB, Kahmen A. 2023. Species and biosynthetic effects
577 cause uncorrelated variation in oxygen and hydrogen isotope compositions of plant organic
578 compounds. Geochimica et Cosmochimica Acta 352:1–13.

579 20. Baan J. 2024. Understanding the metabolic signal in hydrogen isotope values of plant organic
580 compounds. Thesis der Universitat Basel https://doi.org/DOI 10.5451/unibas-ep96717.

581 21. Ladd N, Nelson D, Matthews B, Dyer S, Limberger R, Klatt A, Narwani A, Dubois N, Schubert C.
582 2024. Taxon-specific hydrogen isotope signals in cultures and mesocosms facilitate
583 ecosystem and hydroclimate reconstruction. EarthArXiv https://doi.org/10.31223/X57T30.

584 22. Pilecky M, Kainz MJ, Wassenaar LI. 2024. Exploring hydrogen isotope fractionation in lipid
585 biomolecules of freshwater algae: implications for ecological and paleoenvironmental
586 studies. Isotopes in Environmental and Health Studies 60:585–595.

587 23. Sachs JP, Kawka OE. 2015. The influence of growth rate on 2H/1H fractionation in continuous
588 cultures of the coccolithophorid Emiliania huxleyi and the diatom Thalassiosira pseudonana.
589 PLoS ONE 10:1–27.

24. Van Der Meer MTJ, Benthien A, French KL, Epping E, Zondervan I, Reichart G-J, Bijma J, Sinninghe Damsté JS, Schouten S. 2015. Large effect of irradiance on hydrogen isotope fractionation of alkenones in Emiliania huxleyi. Geochimica et Cosmochimica Acta 160:16–24.

25. Sachs JP, Maloney AE, Gregersen J, Paschall C. 2016. Effect of salinity on 2H/1H fractionation in lipids from continuous cultures of the coccolithophorid Emiliania huxleyi. Geochimica et Cosmochimica Acta 189:96–109.

26. Maloney AE, Shinneman ALC, Hemeon K, Sachs JP. 2016. Exploring lipid 2H/1H fractionation mechanisms in response to salinity with continuous cultures of the diatom Thalassiosira pseudonana. Organic Geochemistry 101:154–165.

27. Wolfshorndl M, Danford R, Sachs JP. 2019. 2H/1H fractionation in microalgal lipids from the North Pacific Ocean: Growth rate and irradiance effects. Geochimica et Cosmochimica Acta 246:317–338.

28. Torres-Romero I, Zhang H, Wijker RS, Clark AJ, McLeod RE, Jaggi M, Stoll HM. 2024. Hydrogen isotope fractionation is controlled by CO_2 in coccolithophore lipids. Proc Natl Acad Sci USA 121:e2318570121.

29. Sachse D, Billault I, Bowen GJ, Chikaraishi Y, Dawson TE, Feakins SJ, Freeman KH, Magill CR, McInerney FA, Van Der Meer MTJ, Polissar P, Robins RJ, Sachs JP, Schmidt HL, Sessions AL, White JWC, West JB, Kahmen A. 2012. Molecular paleohydrology: Interpreting the hydrogen-isotopic composition of lipid biomarkers from photosynthesizing organisms. Annual Review of Earth and Planetary Sciences 40:221–249.

30. Sessions AL. 2016. Factors controlling the deuterium contents of sedimentary hydrocarbons. Organic Geochemistry 96:43–64.

31. Sessions AL, Jahnke LL, Schimmelmann A, Hayes JM. 2002. Hydrogen isotope fractionation in lipids of the methane-oxidizing bacterium Methylococcus capsulatus. Geochimica et Cosmochimica Acta 66:3955–3969.

32. Valentine DL. 2009. Isotopic remembrance of metabolism past. Proceedings of the National Academy of Sciences of the United States of America 106:12565–12566.

33. Zhang X, Gillespie AL, Sessions AL. 2009. Large D/H variations in bacterial lipids reflect central metabolic pathways. Proceedings of the National Academy of Sciences of the United States of America 106:12580–12586.

34. Dawson KS, Osburn MR, Sessions AL, Orphan VJ. 2015. Metabolic associations with archaea drive shifts in hydrogen isotope fractionation in sulfate-reducing bacterial lipids in cocultures and methane seeps. Geobiology 13:462–477.

35. Leavitt WD. 2016. The Inner Lives of Archaea: the hydrogen isotopic composition of Archaeal lipids as a proxy of metabolic state.

36. Osburn MR, Dawson KS, Fogel ML, Sessions AL. 2016. Fractionation of hydrogen isotopes by sulfate- and nitrate-reducing bacteria. Frontiers in Microbiology 7:1–16.

37. Leavitt WD, Murphy SJL, Lynd LR, Bradley AS. 2017. Hydrogen isotope composition of Thermoanaerobacterium saccharolyticum lipids: Comparing wild type with a nfn-transhydrogenase mutant. Organic Geochemistry 113:239–241.

38. Wijker RS, Sessions AL, Fuhrer T, Phan M. 2019. 2H/1H variation in microbial lipids is controlled by NADPH metabolism. Proceedings of the National Academy of Sciences of the United States of America 116:12173–12182.

39. Van de Vossenberg JLCM, Driessen AJM, Konings WN. 1998. The essence of being extremophilic: The role of the unique archaeal membrane lipids. Extremophiles 2:163–170.

40. Schouten S, Hopmans EC, Sinninghe Damsté JS. 2013. The organic geochemistry of glycerol dialkyl glycerol tetraether lipids: A review. Organic Geochemistry 54:19–61.

41. Schouten S, Hopmans EC, SchefuB E, Sinninghe Damsté JS. 2002. Distributional variations in marine crenarchaeotal membrane lipids: a new tool for reconstructing ancient sea water temperatures? Earth and Planetary Science Letters 265–274.

42. Pearson A, Ingalls AE. 2013. Assessing the use of archaeal lipids as marine environmental proxies. Annual Review of Earth and Planetary Sciences 41:359–384.

43. De Rosa M, Gambacorta A. 1988. The lipids of archaebacteria. Progress in Lipid Research 27:153–175.

44. Elling FJ, Könneke M, Lipp JS, Becker KW, Gagen EJ, Hinrichs K-U. 2014. Effects of growth phase on the membrane lipid composition of the thaumarchaeon Nitrosopumilus maritimus and their implications for archaeal lipid distributions in the marine environment. Geochimica et Cosmochimica Acta 141:579–597.

45. Elling FJ, Könneke M, Nicol GW, Stieglmeier M, Bayer B, Spieck E, de la Torre JR, Becker KW, Thomm M, Prosser JI, Herndl GJ, Schleper C, Hinrichs KU. 2017. Chemotaxonomic characterisation of the thaumarchaeal lipidome. Environmental Microbiology 19:2681–2700.

46. Hurley SJ, Elling FJ, Könneke M, Buchwald C, Wankel SD, Santoro AE, Lipp JS, Hinrichs KU, Pearson A. 2016. Influence of ammonia oxidation rate on thaumarchaeal lipid composition and the TEX86 temperature proxy. Proceedings of the National Academy of Sciences of the United States of America 113:7762–7767.

656 47. Cobban A, Zhang Y, Zhou A, Pearson A, Leavitt WD. 2020. Multiple environmental parameters
657 impact core lipid cyclization in Sulfolobus acidocaldarius. Environmental Microbiology 1–28.

658 48. Zhou A, Weber Y, Chiu BK, Elling FJ, Cobban AB, Pearson A, Leavitt WD. 2020. Energy flux
659 controls tetraether lipid cyclization in Sulfolobus acidocaldarius. Environmental Microbiology
660 22:343–353.

661 49. Quehenberger J, Pittenauer E, Allmaier G, Spadiut O. 2020. The influence of the specific
662 growth rate on the lipid composition of Sulfolobus acidocaldarius. Extremophiles 24:413–420.

663 50. Yang W, Chen H, Chen Y, Chen A, Feng X, Zhao B, Zheng F, Fang H, Zhang C, Zeng Z. 2023.
664 Thermophilic archaeon orchestrates temporal expression of GDGT ring synthases in response
665 to temperature and acidity stress. Environmental Microbiology 25:575–587.

666 51. Brock TD, Brock KM, Belly RT, Weiss RL. 1972. Sulfolobus: A new genus of sulfur-oxidizing
667 bacteria living at low pH and high temperature. Archiv Mikrobiol 84:54–68.

668 52. Bischof LF, Haurat MF, Hoffmann L, Albersmeier A, Wolf J, Neu A, Pham TK, Albaum SP, Jakobi
669 T, Schouten S, Neumann-Schaal M, Wright PC, Kalinowski J, Siebers B, Albers S-V. 2019. Early
670 Response of Sulfolobus acidocaldarius to Nutrient Limitation. Front Microbiol 9:3201.

671 53. Quehenberger J, Albersmeier A, Glatzel H, Hackl M, Kalinowski J, Spadiut O. 2017. Sulfolobus
672 – A Potential Key Organism in Future Biotechnology. Frontiers in Microbiology 301:56–67.

673 54. Boyd ES, Pearson A, Pi Y, Li W-J, Zhang YG, He L, Zhang CL, Geesey GG. 2011. Temperature
674 and pH controls on glycerol dibiphytanyl glycerol tetraether lipid composition in the
675 hyperthermophilic crenarchaeon Acidilobus sulfurireducens. Extremophiles 15:59–65.

676 55. Jensen SM, Brandl M, Treusch AH, Ejsing CS. 2015. Structural characterization of ether lipids
677 from the archaeon *Sulfolobus islandicus* by high-resolution shotgun lipidomics: Mapping the
678 lipidome of *Sulfolobus islandicus*. J Mass Spectrom 50:476–487.

679 56. Wagner M, Van Wolferen M, Wagner A, Lassak K, Meyer BH, Reimann J, Albers S-V. 2012.
680 Versatile Genetic Tool Box for the Crenarchaeote Sulfolobus acidocaldarius. Front Microbio 3.

681 57. Zhang YG, Pagani M, Wang Z. 2016. Ring Index: A new strategy to evaluate the integrity of TEX
682 $_{86}$ paleothermometry. Paleoceanography 31:220–232.

683 58. Abrahim A, Cannavan A, Kelly SD. 2020. Stable isotope analysis of non-exchangeable
684 hydrogen in carbohydrates derivatised with N-methyl-bis-trifluoroacetamide by gas
685 chromatography – Chromium silver reduction/High temperature Conversion-isotope ratio
686 mass spectrometry (GC-CrAg/HTC-IRMS). Food Chemistry 318:126413.

687 59. Kopf S, Davidheiser-Kroll B, Kocken I. 2021. Isoreader: An R package to read stable isotope
688 data files for reproducible research. JOSS 6:2878.

689 60. Harris, C. 2025. Datasets and code for: Lipid hydrogen isotope compositions primarily reflect
690 growth water in the model archaeon Sulfolobus acidocaldarius (v.1.0.0).
691 Zenodo. https://doi.org/10.5281/zenodo.14743998

692 61. Lewis AM, Recalde A, Bräsen C, Counts JA, Nussbaum P, Bost J, Schocke L, Shen L, Willard
693 DJ, Quax TEF, Peeters E, Siebers B, Albers S-V, Kelly RM. 2021. The biology of
694 thermoacidophilic archaea from the order Sulfolobales. FEMS Microbiology Reviews 1–60.

695 62. Reysenbach A-L, Cady SL. 2001. Microbiology of ancient and modern hydrothermal systems.
696 Trends in Microbiology 9:79–86.

697 63. Auernik KS, Cooper CR, Kelly RM. 2008. Life in hot acid: pathway analyses in extremely
698 thermoacidophilic archaea. Current Opinion in Biotechnology 19:445–453.

699 64. Siliakus MF, Van Der Oost J, Kengen SWM. 2017. Adaptations of archaeal and bacterial
700 membranes to variations in temperature, pH and pressure. Extremophiles 21:651–670.

701 65. Jia B, Liu J, Van Duyet L, Sun Y, Xuan YH, Cheong G-W. 2015. Proteome profiling of heat,
702 oxidative, and salt stress responses in Thermococcus kodakarensis KOD1. Front Microbiol 6.

703 66. Sachs JP, Schwab VF. 2011. Hydrogen isotopes in dinosterol from the Chesapeake Bay
704 estuary. Geochimica et Cosmochimica Acta 75:444–459.

705 67. Thauer RK, Kaster A-K, Seedorf H, Buckel W, Hedderich R. 2008. Methanogenic archaea:
706 ecologically relevant differences in energy conservation. Nat Rev Microbiol 6:579–591.

707 68. Spaans SK, Weusthuis RA, Van Der Oost J, Kengen SWM. 2015. NADPH-generating systems in
708 bacteria and archaea. Front Microbiol 6.

709 69. Wakagi T, Oshima T. 1987. Energy metabolism of a thermoacidophilic
710 archaebacterium,Sulfolobus acidocaldarius. Origins Life Evol Biosphere 17:391–399.

711 70. Liu L-J, Jiang Z, Wang P, Qin Y-L, Xu W, Wang Y, Liu S-J, Jiang C-Y. 2021. Physiology, Taxonomy,
712 and Sulfur Metabolism of the Sulfolobales, an Order of Thermoacidophilic Archaea. Front
713 Microbiol 12:768283.

714 71. Valentine DL. 2007. Adaptations to energy stress dictate the ecology and evolution of the
715 Archaea. Nature Reviews Microbiology 5:316–323.

716 72. Bräsen C, Esser D, Rauch B, Siebers B. 2014. Carbohydrate Metabolism in Archaea: Current
717 Insights into Unusual Enzymes and Pathways and Their Regulation. Microbiol Mol Biol Rev
718 78:89–175.

719 73. Schouten S, Ossebaar J, Schreiber K, Kienhuis MVM, Langer G, Benthien A, Bijma J. 2006. The
720 effect of temperature, salinity and growth rate on the stable hydrogen isotopic composition of
721 long chain alkenones produced by Emiliania huxleyi and Gephyrocapsa oceanica.
722 Biogeosciences 3:113–119.

723 74. Zhang Z, Sachs JP, Marchetti A. 2009. Hydrogen isotope fractionation in freshwater and
724 marine algae: II. Temperature and nitrogen limited growth rate effects. Organic Geochemistry
725 40:428–439.

726 75. Quehenberger J, Albersmeier A, Glatzel H, Hackl M, Kalinowski J, Spadiut O. 2019. A defined
727 cultivation medium for Sulfolobus acidocaldarius. Journal of Biotechnology 301:56–67.

728 76. Harris C, Rhim J, Zhang Y, Cobban A, McFarlin J, Batther H, Kopf S, Leavitt W. 2022.
729 Determining controls on hydrogen isotope fractionation in archaeal tetraether lipids in a
730 thermoacidophilic archaeal heterotrophGoldschmidt2022 abstracts. European Association
731 of Geochemistry, Honolulu, HI, USA.

732 77. Nunn CEM, Johnsen U, Schönheit P, Fuhrer T, Sauer U, Hough DW, Danson MJ. 2010.
733 Metabolism of Pentose Sugars in the Hyperthermophilic Archaea Sulfolobus solfataricus and
734 Sulfolobus acidocaldarius. Journal of Biological Chemistry 285:33701–33709.

735 78. Campbell BJ, Li C, Sessions AL, Valentine DL. 2009. Hydrogen isotopic fractionation in lipid
736 biosynthesis by H2-consuming Desulfobacterium autotrophicum. Geochimica et
737 Cosmochimica Acta 73:2744–2757.

738 79. Zhang Z, Sachs JP. 2007. Hydrogen isotope fractionation in freshwater algae: I. Variations
739 among lipids and species. Organic Geochemistry 38:582–608.

740

Tables

Table 1. Summary of culture conditions and descriptive growth statistics for S. acidocaldarius grown over varying environmental conditions. δ^2H_W is the H-isotope composition of media water at the time of lipid sampling. *Growth d*ata for batch and fed-batch environmental condition experiments were initially reported in Cobban et al., (2020), *growth* data for chemostat experiment was initially reported in Zhou et al., (2019). *For batch experiments, RPM is shaking rate; for bioreactor experiments, RPM is impellor speed.

Table 2. Descriptive statistics for individual biphytanyl (BP) lipids derived from iGDGTs for *S. acidocaldarius* grown under varying environmental conditions. Mean and sd include biological replication (N ≥ 1) and technical replication (e.g., multiple injections, n ≥ 3). Abundance-weighted means are shown for δ^2H_{BP}, $^2\varepsilon_{L/W}$, and Δε/ring values with propagated error.

Figures

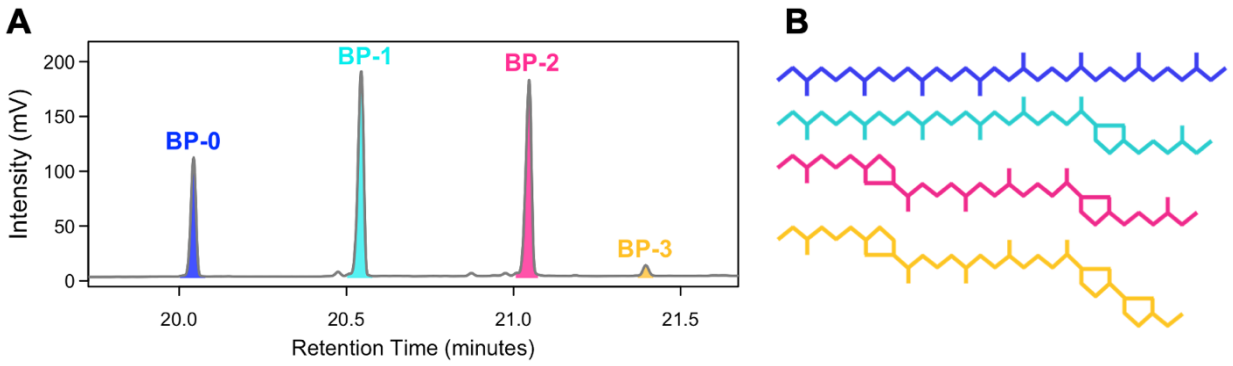

Fig 1. (A) Representative chromatogram of intensity vs. retention time for four iGDGT-derived biphytane (BP) moieties identified in *S. acidocaldarius* biomass that are named for the number of cyclopentane rings they contain. Although a BP-3 peak was detected, in many cases it is present in too low quantities to perform isotopic measurements **(B)** The identity and structure of BP-0 to BP-3.

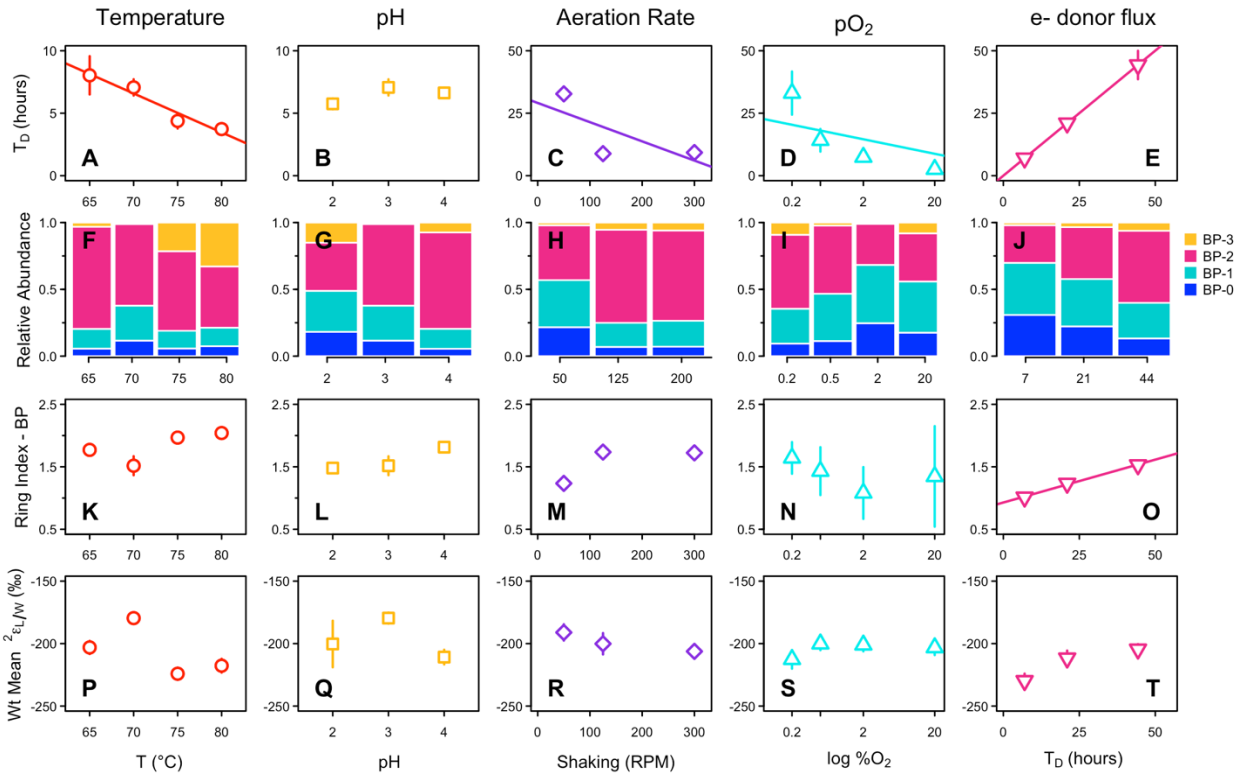

Fig. 2. Results for *S. acidocaldarius* grown under varying environmental conditions. Top row (**A-E**): Doubling time in response to each environmental condition. Second row (**F-J**): Relative abundance of biphytane (BP) lipids derived from iGDGTs. BP-3 was the least abundant and was below the detection limit in some samples. Bars represent the mean across replicates for each treatment level. Third row (**K-O**): Ring Index (RI-BP) of biphytane lipids derived from iGDGTs. Bottom row (**P-T**) The abundance weighted mean H-isotope fractionation ($^{2}\varepsilon_{L/W}$) between growth water and biphytanes. For all rows, points represent the mean and propagated error across biological and technical replicates for each treatment level. In many cases, error bars are smaller than symbols. Only statistically significant regressions are shown ($p < 0.05$).

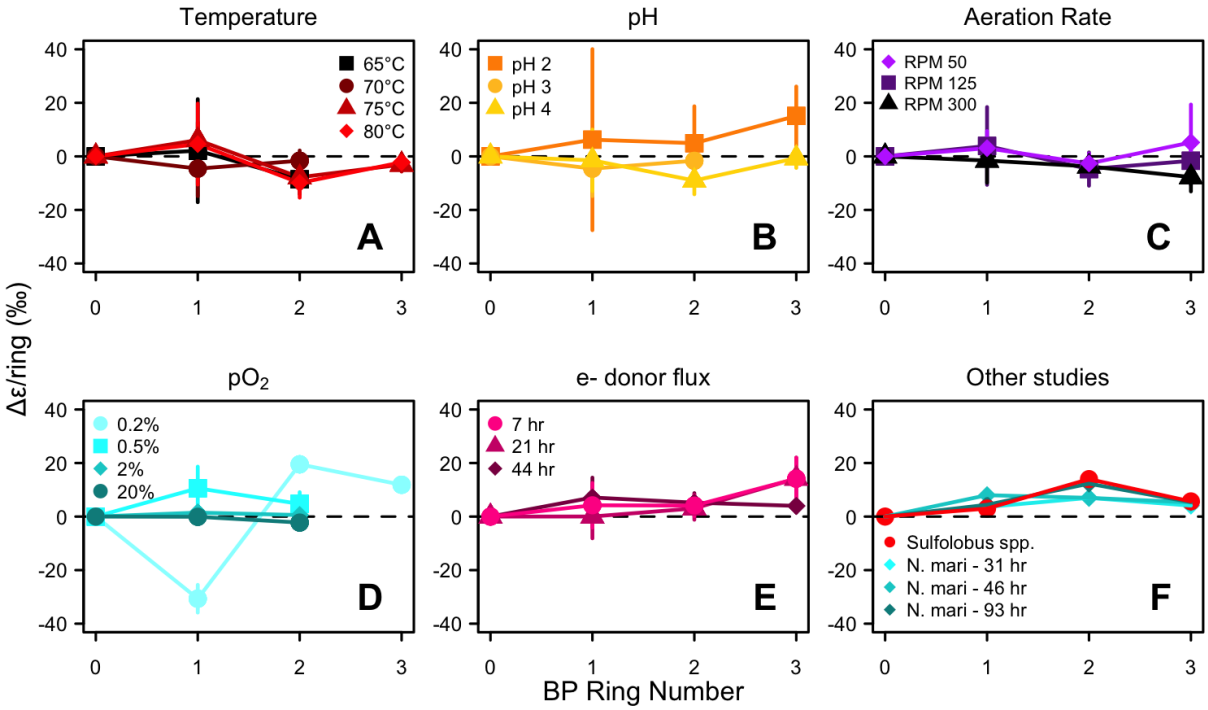

Fig. 3. (**A-E**) Ring difference (Δε/ring, ‰) for individual biphytanes in each environmental condition experiment. BP-0 has a Δε/ring of 0 by definition and is shown for reference. BP-3 was not recovered from every treatment. Note the axes are scaled differently for each plot. Points represent mean of biological and technical replicates for each treatment level. (**F**) Ring difference for biphytanes examined in other studies. Blue diamonds are *N. maritimus* from Leavitt et al., 2023; red squares are *Sulfolobus* sp. from Kaneko et al., 2011. Kaneko et al., also recovered BP-4 from *Sulfolobus* spp. (data not shown); the Δε/ring for BP-4 is 11.7 ‰.

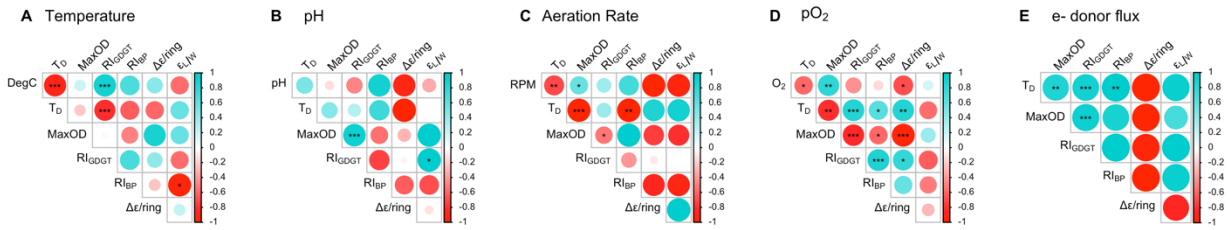

Fig. 4. Correlation matrices showing linear relationships among environmentally manipulated parameters, growth statistics (doubling time (T_D) and maximum OD_{600}), mean cyclization of lipids (RI-GDGT and RI-BP), ring difference, and abundance weighted mean $^2\varepsilon_{L/W}$ for (**A**) temperature, (**B**) pH, (**C**) aeration rate, (**D**) O_2 mixing ratio, and (**E**) electron donor flux. Notably, mean $^2\varepsilon_{L/W}$ values do not show a strong linear correlation to any other measured parameter, indicating that environmental conditions, growth statistics, and mean cyclization do not significantly influence the degree of lipid/water fractionation in *S. acidocaldarius*. Circle color and size indicate the strength and direction (blue = correlated, red = anticorrelated) of the relationship. Significance levels: * $p < 0.05$, ** $p < 0.001$, *** $p < 0.0001$. Circles without a star indicate the relationship is not statistically significant.

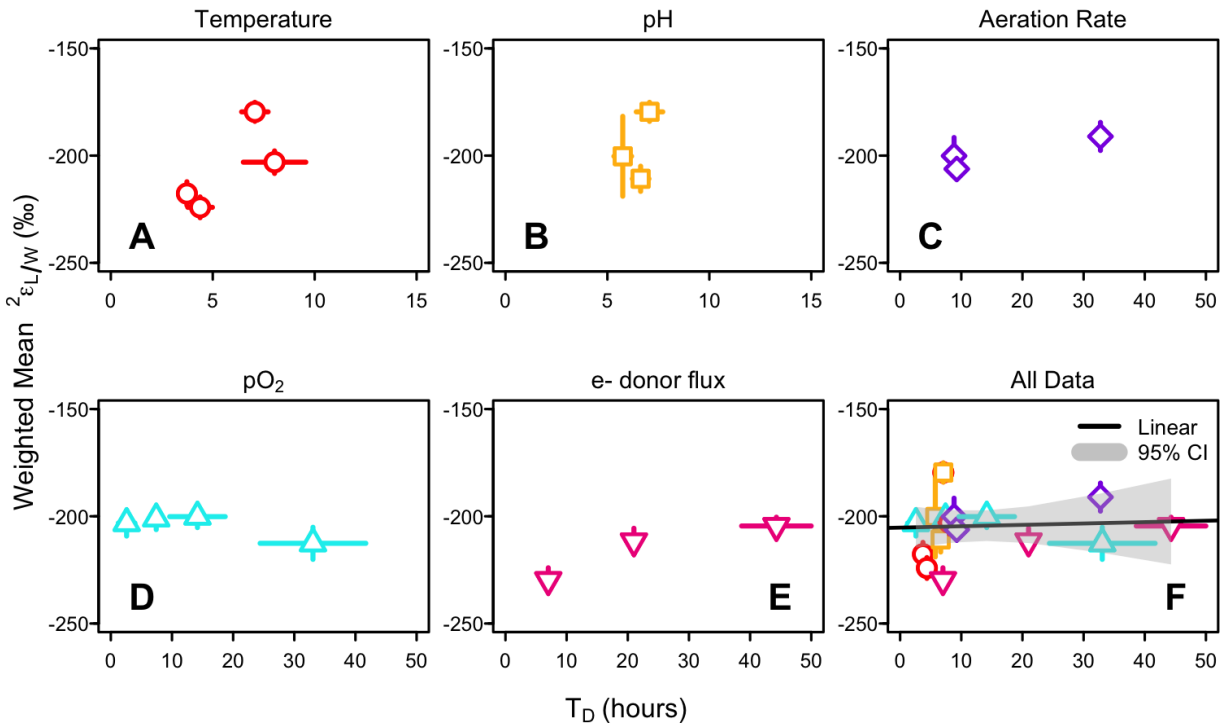

Fig. 5. The abundance weighted H-isotope fractionation ($^{2}\varepsilon_{L/W}$) between growth water and biphytanes (BPs) in response to doubling time (hours) in each individual environmental condition experiment (**A-E**) and pooled across all experiments (**F**). When data from all environmental control experiments is pooled, there is no relationship between doubling time (hours) and abundance weighted mean $^{2}\varepsilon_{L/W}$. Points represent mean of biological and technical replicates for each treatment level. Error bars represent propagated error associated with BP abundance measurements, BP-δ^{2}H measurements, and weighted mean $^{2}\varepsilon_{L/W}$ calculations; bars are smaller than the symbols in many cases.

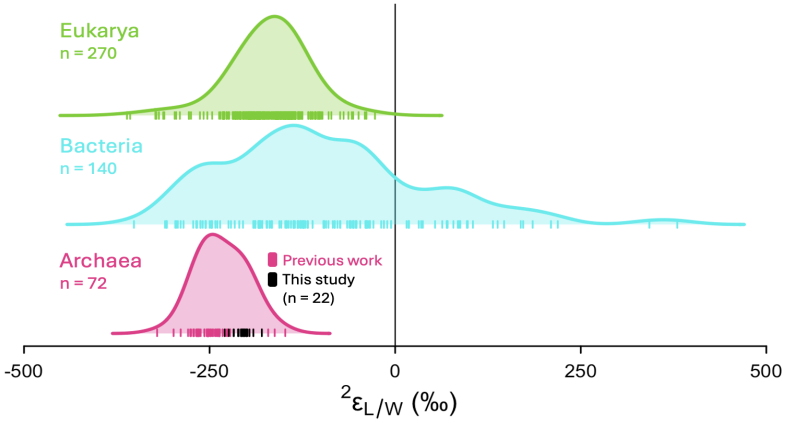

Fig. 6. Summary of lipid/water fractionation ($^2\varepsilon_{L/W}$) in culture studies across three domains of life: eukaryotic phototrophs (green; n = 270), bacteria (blue; n = 140), and archaea (pink; n = 72). Tick marks indicate individual $^2\varepsilon_{L/W}$ values; shaded curves indicate probability density functions. Archaea data includes measurements of phytanes and biphytanes from *Sulfolobus* sp. (Kaneko et al., 2011), *M. barkeri* (Wu et al., 2020), *N. maritimus* (Leavitt et al., 2022), *Acidianus* sp. DS80, *A. fulgidus*, and *Metallosphaera sedula* (Rhim et al., 2024), and *S. acidocaldarius* (this study; black tick marks). Data for Eukarya and Bacteria is redrawn from Rhim et al., (2024), Figure 6. Eukarya data includes measurements for acetogenic and isoprenoid lipids. Bacteria data includes fatty acids synthesized by multiple metabolisms (e.g., aerobic and anaerobic heterotrophy, aerobic and anaerobic chemoautotrophy, and photoautotrophy).